Three-dimensional control of crystal growth using magnetic fields

George S. Dulikravich and Vineet Ahuja

The Pennsylvania State University, Department of Aerospace Engineering
233 Hammond Building, University Park, PA 16802, USA
and

Seungsoo Lee

Agency for Defense Development, Aerodynamics Research Department
Taejon, Republic of Korea

ABSTRACT

Two coupled systems of partial differential equations governing three-dimensional laminar viscous flow undergoing solidification or melting under the influence of arbitrarily oriented externally applied magnetic fields have been formulated. The model accounts for arbitrary temperature dependence of physical properties including latent heat release, effects of Joule heating, magnetic field forces and mushy region existence. On the basis of this model a numerical algorithm has been developed and implemented using central differencing on a curvilinear boundary-conforming grid and Runge-Kutta explicit time-stepping. The numerical results clearly demonstrate possibilities for active and practically instantaneous control of melt/solid interface shape, the solidification/melting front propagation speed, and the amount and location of solid accrued.

Nomenclature

c	= specific heat, J kg^{-1} K^{-1}
Ec	= Eckert number
Fr	= Froude number
g	= gravity force per unit mass, m s^{-2}
Gr	= Grashof number
H	= (H_x, H_y, H_z) = magnetic field, H kg^{-1}
H_t	= Hartmann number
k	= heat conductivity coeff., W m^{-1} K^{-1}
l	= length, m
L	= latent heat of liquid/solid change, J kg^{-1}
p	= pressure, kg m^{-1} s^{-2}
P_m	= magnetic Prandtl number
Pr	= Prandtl number
Ra	= Gr Pr = Rayleigh number
Re	= hydrodynamic Reynolds number
R_m	= Re P_m = magnetic Reynolds number
R	= volume fraction of the liquid phase
S_{te}	= Stefan number
t	= time, s
T	= absolute temperature, K
ΔT	= characteristic temperature diff., K
v	= (u,v,w) = velocity vector, m s^{-1}
x,y,z	= Cartesian coordinates, m
α	= thermal expansion coefficient, K^{-1}
β	= artificial compressibility parameter
θ	= nondimensional temperature
ρ	= density, kg m^{-3}
η	= viscosity coefficient, kg m^{-1} s^{-1}
ξ, η, ζ	= non-orthogonal grid-following coordinates, m
μ	= magnetic permeability, H m^{-1}
σ	= electrical conductivity, Ω^{-1} m^{-1}
ϕ	= gravity potential ($g_i = \phi_{,i}$)

subscripts

e	= equivalent
l	= liquidus
o	= reference values
s	= solidus

superscripts

*	= nondimensional values
'	= function of nondimensional temperature

0-8194-1149-3/93/$6.00

1. INTRODUCTION

In the field of a large single crystal growth from a melt it is highly desireable to control the process using non-intrusive means having a very fast response time. For example, in a Czochralski crystal growth it is possible to vary the outside wall temperature of the container. In this case the response time is of the order of an hour thus making this control approach inappropriate. Instead, it is possible to use a magnetic field[1-6] or an electric field[7] to control the melt motion almost instantaneously[8]. It has been well known[9] that the magnetic field can eliminate vorticity from the flow field and even suppress any fluid motion so that the solid/liquid front shape, its propagation speed and the amount of accrued solid could be manipulated. Recent applications of the magnetic fields to solidifying melts have been either in the radial[10] or in the axial[11,12] direction without a clear understanding or a capability to study a fully three-dimensional orientation of the magnetic field. The objective of this paper is to briefly expose a mathematical model and an accompanying numerical algorithm that are capable of simulating fully three-dimensional melt flow control during melting and solidification via an arbitrarily oriented externally applied steady magnetic field. The formulation presented in this paper simultaneously predicts detailed velocity, pressure, temperature and magnetic field for the moving melt, while capturing the forming solid phase with a single computer code.

2. ANALYTICAL MODEL

The sets of the fluid flow partial differential equations (Navier-Stokes) and the magnetic field transport partial differential equations (Maxwell) can be non-dimensionalized as follows

$$v_i^* = \frac{v_i}{v_o} \qquad x_i^* = \frac{x_i}{l_o} \qquad t^* = \frac{t\, v_o}{l_o} \qquad p^* = \frac{p}{\rho_o\, v_o^2} \tag{1}$$

$$g^* = \frac{g_i}{g_o} \qquad H_i^* = \frac{H_i}{H_o} \qquad \theta = \frac{T - T_o}{\Delta T} \qquad \sigma^* = \frac{\sigma}{\sigma_o} \qquad \mu^* = \frac{\mu}{\mu_o} \tag{2}$$

where we chose $T_o = T_s$. Thermal buoyancy was incorporated via an extended[13,14] Boussinesq approximation which allows for fluid properties that vary as arbitrary functions of temperature. Thus,

$$\rho = \rho_o\, \rho'(\theta) \qquad c = c_o\, c'(\theta) \qquad \eta = \eta_o\, \eta'(\theta) \qquad k = k_o\, k'(\theta) \qquad \sigma = \sigma_o \qquad \mu = \mu_o \tag{3}$$

$$\rho' = 1 + \left.\frac{\partial(\rho/\rho_o)}{\partial\theta}\right|_o \theta_s + \left.\frac{\partial(\rho/\rho_o)}{\partial\theta}\right|_s (\theta - \theta_s) = 1 - \alpha_o^*\theta_s - \alpha_s^*(\theta - \theta_s) = 1 - (\alpha_o^* - \alpha_s^*)\theta_s - \alpha_s^*\theta \tag{4}$$

with a similar expression for k' . Using the following non-dimensional groups

$$Re = \frac{\rho_o\, v_o\, l_o}{\eta_o} \qquad Fr^2 = \frac{v_o^2}{g_o\, l_o} \qquad Ec = \frac{v_o^2}{c_o\, \Delta T} \qquad Pr = \frac{\eta_o\, c_o}{k_o} \qquad Gr = \frac{\rho_o^2\, \alpha_o\, g_o\, \Delta T\, l_o^3}{\eta_o^2} \tag{5}$$

$$Ra = Gr\,Pr \qquad S_{te} = \frac{c_o\,\Delta T}{L} \qquad P_m = \frac{\mu_o\,\sigma_o\,\eta_o}{\rho_o} \qquad R_m = Re\,P_m \qquad H_t = \mu_o\,l_o\,H_o\left(\frac{\sigma_o}{\eta_o}\right)^{1/2} \quad (6)$$

assuming that $\alpha_s{}^*\theta << 1$ and dropping the asterisk symbol, the governing equations become

$$v_{i,i} = 0 \quad (7)$$

$$v_{i,t} + (v_i\,v_j)_{,j} = \frac{1}{Re}(\eta'\,v_{i,j})_{,j} - \bar{\bar{p}}_{,i} + \frac{R\,Gr\,\theta}{Re^2}g_i + \frac{H_t{}^2}{P_m Re^2}(H_i\,H_k)_{,k} \quad (8)$$

$$\theta_{,t} + v_i\,\theta_{,i} = \frac{R}{Re\,Pr\,c_e'}(k_l'\,\theta_{,i})_{,i} + \frac{(1-R)}{Re\,Pr\,c_e'}(k_s'\,\theta_{,i})_{,i} + \frac{H_t{}^2\,Ec}{c_e'\,P_m{}^2\,R_e{}^3}\varepsilon_{ijk}\varepsilon_{ilm}\,H_{k,j}\,H_{m,l} \quad (9)$$

$$H_{,t} - (v_j\,H_i - v_i\,H_j)_{,j} = \frac{1}{P_m\,R_e}H_{i,jj} \quad (10)$$

where the last equation represents three components of the non-dimensional magnetic field transport conservation. Non-dimensional hydrostatic, hydrodynamic, and magnetic pressures were combined to give

$$\bar{\bar{p}} = p + \frac{\phi}{Fr^2} + \frac{H_t{}^2}{P_m Re^2}H_iH_i \quad (11)$$

The latent heat released/absorbed per unit mass of mushy region ($T_l > T > T_s$) is proportional to the local volumetric liquid/solid ratio often modeled[14] as

$$R = \frac{V_l}{V_l + V_s} = \left(\frac{\theta - \theta_s}{\theta_l - \theta_s}\right)^n \quad (12)$$

where $0.2 < n < 5$. Let $S = 1$ for a fully molten cell and $S = 0$ for a fully solid cell. Then the non-dimensional equivalent specific heat, $c_e' = c_e / c_o$, involving continuous influence of the latent heat can be generalized as

$$c_e' = \left(R\,c_l' - \frac{S}{S_{te}}\frac{\partial R}{\partial \theta}\rho_l'\right) + \left((1-R)\,c_s' + \frac{(1-S)}{S_{te}}\frac{\partial R}{\partial \theta}\rho_s'\right) \quad (13)$$

3. NUMERICAL MODEL

Equations (7-9) represent a system of five coupled non-linear non-dimensional partial differential equations (Navier-Stokes) for incompressible flows with possible solidification or melting. These can be written in a fully conservative form in terms of the non-orthogonal grid-following boundary-fitted coordinate system as

$$\frac{\partial \tilde{\mathbf{Q}}}{\partial t} + \frac{\partial \tilde{\mathbf{E}}}{\partial \xi} + \frac{\partial \tilde{\mathbf{F}}}{\partial \eta} + \frac{\partial \tilde{\mathbf{G}}}{\partial \zeta} = \tilde{D}^2 + \tilde{\mathbf{S}} \quad (14)$$

where $\tilde{Q}$ is the solution vector and $\tilde{E}$, $\tilde{F}$ and $\tilde{G}$ are the transformed flux vectors. Let $J = \det\left[\frac{\partial(\xi,\eta,\zeta)}{\partial(x,y,z)}\right]$ be the Jacobian determinant of the geometric transformation matrix. The vectors are defined as follows

$$\tilde{Q}=\frac{1}{J}\begin{Bmatrix} \left(\frac{\bar{\bar{p}}}{\beta J}\right) \\ u \\ v \\ w \\ \theta \end{Bmatrix} \quad \tilde{E}=\frac{1}{J}\begin{Bmatrix} U \\ Uu+\xi_{,x}\,\bar{\bar{p}} \\ Uv+\xi_{,y}\,\bar{\bar{p}} \\ Uw+\xi_{,z}\,\bar{\bar{p}} \\ U\theta \end{Bmatrix} \quad \tilde{F}=\frac{1}{J}\begin{Bmatrix} V \\ Vu+\eta_{,x}\,\bar{\bar{p}} \\ Vv+\eta_{,y}\,\bar{\bar{p}} \\ Vw+\eta_{,z}\,\bar{\bar{p}} \\ V\theta \end{Bmatrix} \quad \tilde{G}=\frac{1}{J}\begin{Bmatrix} W \\ Wu+\zeta_{,x}\,\bar{\bar{p}} \\ Wv+\zeta_{,y}\,\bar{\bar{p}} \\ Ww+\zeta_{,z}\,\bar{\bar{p}} \\ W\theta \end{Bmatrix} \tag{15}$$

The diffusion vector in general curvilinear coordinates is defined as

$$\tilde{D}^2 = \bar{\bar{D}}\left[\frac{\tilde{D}}{J} g_{ij} \left(J\tilde{Q}\right)_{,j}\right]_{,i} \quad \text{with the metric tensor defined as} \quad g_{ij} = \frac{\partial \bar{x}_i}{\partial \hat{x}_j}\frac{\partial \bar{x}_j}{\partial \hat{x}_i} \tag{16}$$

$$\bar{\bar{D}} = \mathrm{diag}\left[0 \ \frac{R}{Re} \ \frac{R}{Re} \ \frac{R}{Re} \ \left\{\frac{R}{RePr\, c_e'} \quad \frac{(1-R)}{RePr\, c_e'}\right\}\right] \qquad \tilde{D} = \mathrm{diag}\left[0 \ \frac{\eta'}{J} \ \frac{\eta'}{J} \ \frac{\eta'}{J} \ \begin{Bmatrix} k_l'/J \\ k_s'/J \end{Bmatrix}\right] \tag{17}$$

The contravariant components U, V, W and $\hat{H}_\xi$, $\hat{H}_\eta$, $\hat{H}_\zeta$ are defined as

$$\begin{Bmatrix} U \\ V \\ W \end{Bmatrix} = \begin{bmatrix} \xi_{,x} & \xi_{,y} & \xi_{,z} \\ \eta_{,x} & \eta_{,y} & \eta_{,z} \\ \zeta_{,x} & \zeta_{,y} & \zeta_{,z} \end{bmatrix} \begin{Bmatrix} u \\ v \\ w \end{Bmatrix} \qquad \begin{Bmatrix} \hat{H}_\xi \\ \hat{H}_\eta \\ \hat{H}_\zeta \end{Bmatrix} = \begin{bmatrix} \xi_{,x} & \xi_{,y} & \xi_{,z} \\ \eta_{,x} & \eta_{,y} & \eta_{,z} \\ \zeta_{,x} & \zeta_{,y} & \zeta_{,z} \end{bmatrix} \begin{Bmatrix} H_x \\ H_y \\ H_z \end{Bmatrix} \tag{18}$$

Since there is no physical time derivative term in the mass conservation equation, an artificial compressibility[15] term, $\frac{\partial}{\partial t}\left(\frac{\bar{\bar{p}}}{\beta J}\right)$, was added to the mass conservation so that the system (14) can be integrated simultaneously. In the steady state limit, the time variation of the $\tilde{Q}_1$ term tends to zero and does not influence the accuracy of the steady state solution.The non-zero components[16] of the source vector $\tilde{S}$ are

$$\tilde{S}_2 = \frac{H_t^2}{P_m\, Re^2}\left(\frac{\partial}{\partial\xi}\left(\frac{\hat{H}_\xi\, H_x}{J}\right) + \frac{\partial}{\partial\eta}\left(\frac{\hat{H}_\eta\, H_x}{J}\right) + \frac{\partial}{\partial\zeta}\left(\frac{\hat{H}_\zeta\, H_x}{J}\right)\right) - \frac{R\, Gr\, \theta}{Re^2 J} g_x \tag{19}$$

$$\tilde{S}_3 = \frac{H_t^2}{P_m\, Re^2}\left(\frac{\partial}{\partial\xi}\left(\frac{\hat{H}\xi\, H_y}{J}\right) + \frac{\partial}{\partial\eta}\left(\frac{\hat{H}\eta\, H_y}{J}\right) + \frac{\partial}{\partial\zeta}\left(\frac{\hat{H}\zeta\, H_y}{J}\right)\right) - \frac{R\, Gr\, \theta}{Re^2 J}\, g_y \tag{20}$$

$$\tilde{S}_4 = \frac{H_t^2}{P_m\, Re^2}\left(\frac{\partial}{\partial\xi}\left(\frac{\hat{H}\xi\, H_z}{J}\right) + \frac{\partial}{\partial\eta}\left(\frac{\hat{H}\eta\, H_z}{J}\right) + \frac{\partial}{\partial\zeta}\left(\frac{\hat{H}\zeta\, H_z}{J}\right)\right) - \frac{R\, Gr\, \theta}{Re^2 J}\, g_z \tag{21}$$

$$\tilde{S}_5 = \frac{J}{c_e}\frac{H_t^2 Ec}{R_m^2\, Re}\left(\tilde{P}_1^2 + \tilde{P}_2^2 + \tilde{P}_3^2\right) \tag{22}$$

where

$$\tilde{P}_1 = \frac{\partial}{\partial\xi}\left(\frac{H_z\xi_{,y} - H_y\xi_{,z}}{J}\right) + \frac{\partial}{\partial\eta}\left(\frac{H_z\eta_{,y} - H_y\eta_{,z}}{J}\right) + \frac{\partial}{\partial\zeta}\left(\frac{H_z\zeta_{,y} - H_y\zeta_{,z}}{J}\right) \tag{23}$$

$$\tilde{P}_2 = \frac{\partial}{\partial\xi}\left(\frac{H_x\xi_{,z} - H_z\xi_{,x}}{J}\right) + \frac{\partial}{\partial\eta}\left(\frac{H_x\eta_{,z} - H_z\eta_{,x}}{J}\right) + \frac{\partial}{\partial\zeta}\left(\frac{H_x\zeta_{,z} - H_z\zeta_{,x}}{J}\right) \tag{24}$$

$$\tilde{P}_3 = \frac{\partial}{\partial\xi}\left(\frac{H_y\xi_{,x} - H_x\xi_{,y}}{J}\right) + \frac{\partial}{\partial\eta}\left(\frac{H_y\eta_{,x} - H_x\eta_{,y}}{J}\right) + \frac{\partial}{\partial\zeta}\left(\frac{H_y\zeta_{,x} - H_x\zeta_{,y}}{J}\right) \tag{25}$$

For the transformed system of three magnetic field transport equations the solution vector $\tilde{\mathbf{Q}}$, the flux vectors, $\tilde{\mathbf{E}}$, $\tilde{\mathbf{F}}$, $\tilde{\mathbf{G}}$, and the matrix, $\tilde{\mathbf{D}}$, are defined as

$$\tilde{Q}=\frac{1}{J}\begin{Bmatrix} H_x \\ H_y \\ H_z \end{Bmatrix} \quad \tilde{E}=\frac{1}{J}\begin{Bmatrix} H_xU-u\hat{H}\xi \\ H_yU-v\hat{H}\xi \\ H_zU-w\hat{H}\xi \end{Bmatrix} \quad \tilde{F}=\frac{1}{J}\begin{Bmatrix} H_xV-u\hat{H}\eta \\ H_yV-v\hat{H}\eta \\ H_zV-w\hat{H}\eta \end{Bmatrix} \quad \tilde{G}=\frac{1}{J}\begin{Bmatrix} H_xW-u\hat{H}\zeta \\ H_yW-v\hat{H}\zeta \\ H_zW-w\hat{H}\zeta \end{Bmatrix} \quad \tilde{D}=\frac{1}{P_m\, Re}\,I \tag{26}$$

while $\tilde{\tilde{D}}= I$ and $\tilde{S} = 0$. Thus, for simulation of a fully three-dimensional MagnetoHydroDynamic (MHD) flows with phase change it is neccessary to simultaneously integrate eight partial differential equations by transferring the information through source-like terms[16].

4. NUMERICAL RESULTS

An explicit four-stage Runge-Kutta time-stepping algorithm[17] and a central finite difference spatial discretization were used for the iterative solution of system (14) for both Navier-Stokes and magnetic transport equations over the entire domain occupied by both the melt and the solid. A simple cubical closed container (Fig. 1) filled with molten silicon (Table 1) was chosen as the common test configuration where the computational grid conforms with the original walls of the container. Physical properties of silicon have

been compiled from various publications[18-20]. The grid consisted of 20 x 20 x 20 grid cells that were symmetrically clustered towards the solid walls of the container. Velocity components on these walls were specified as zero and the pressure was computed from the normal momentum equation at the wall. A uniform unidirectional magnetic field was specified on all walls thus treating the walls as magnetically conducting. This formulation simultaneously predicts detailed velocity, pressure, magnetic and temperature fields for the moving melt while capturing the mushy region and the forming solid phase by using a single computer code. The same computer code can simulate the reverse process of thawing or melting of the solids. In all of the computer test runs we used Courant-Friedrichs-Levy (CFL) number of 2.8, von Neuman number of 0.4, artificial compressibility parameter β of 10 and artificial fourth order dissipation[17] coefficient of 0.0056. The values of the reference quantities were: $v_o = 0.02269$ m s^{-1}, $l_o = 0.01$ m, $\Delta T = 37.5$ K, $\rho_o = 2550$ kg m^{-3}, $c_o = 1059$ J kg^{-1} K^{-1}, $k_o = 64$ W m^{-1} K^{-1}, $T_o = 1685$ K, $\eta_o = 7.018 \times 10^{-4}$ kg m^{-1} s^{-1}, $\sigma_o = 4.3 \times 10^4$ W^{-1} m^{-1} and $g_o = 9.81$ m s^{-2}. We used a simple linear variation of the solid fraction, S, in the mushy region, that is, $S = (T - T_S) / (T_l - T_S)$. It should also be pointed out that the values of c, k and η were varied linearly within the mushy region. The exponent in equation (13) was n = 5 in all runs. Notice (Table 2) that we have assumed that the magnetic permeability coefficient for silicon is one order of magnitude larger than for vacuum. Consequently, the Hartmann number in our case becomes $Ht = 418.6\ B_o$, where B_o is the magnetic field strength measured in Teslas. In all pertinent cases we used Ht = 100 corresponding to $B_o = 0.2389$ Tesla. All computations were performed in Fortran language on a Cray-YMP computer using a single processor. A typical computation time was approximately half an hour. In all test cases the vertical wall at x = 0 was kept uniformly hot ($\theta = 2$) and the opposite vertical wall at x = 1 was kept uniformly cold ($\theta = -1$), while the remaining walls were thermally isolated. Uniform gravity was applied in the negative z-direction (Fig. 1) in all the test cases. Following is the discussion of the computational results obtained by orientating a uniform steady external magnetic field along different axes. Depending on the orientation of the magnetic field, different amount of solid phase has accrued (Fig. 2) in each of the test cases.

4.1 Solidification with no magnetic field:

Comparison of the computed isotherms (Fig. 3a) in the vertical mid-plane (y = 0.5) and the velocity vector field (Fig. 3b) in the same plane give a clear picture of the strong melt circulatory flow and the solid that accrued on the cold wall (x = 1). Notice that the liquid/solid interface is highly curved in this plane and there are strong thermal gradients in the solid accrued on the cold vertical wall (resulting in 1666 solidified cells). Similarly, computed isotherms (Fig. 3c) in the horizontal mid-plane (z = 0.5) show that the thermal gradients inside the solid are significant and the solid/liquid shape do not vary significantly in the y-direction.

4.2 Solidification with magnetic field in y-direction (perpendiculat to plane of recirculation):

Computed isotherms (Fig.4a) in the vertical mid-plane (y = 0.5) when compared with the isotherms in the case without the magnetic field (Fig. 3a) appear to be less curved and the vertical thermal boundary layer is thicker. As expected, the computed velocity vector field (Fig. 4b) in the same plane is clearly weaker than the computed velocity field in the case without the magnetic field (Fig. 3b). Consequently, more solid accrued when the magnetic field was applied (resulting in 1843 solidified cells) and the liquid/solid interface straightened somewhat. Since the magnetic field reduced melt convection, the computed isotherms in the horizontal mid-plane (z = 0.5) show almost no variation (Fig. 4c) in the y-direction.

4.3 Solidification with magnetic field in x-direction (from hot to cold wall):

In this case the magnetic field is acting in the hot-to-cold wall direction. The computed isotherms (Fig.5a) in the vertical mid-plane (y = 0.5) when compared with the isotherms in the case with the magnetic field acting

in y-direction (Fig. 4a) are significantly straightened. The magnetic field acting perpendicular to the hot and the cold vertical walls is definitely suppressing the melt motion (Fig. 5b) as was observed by other researchers [9]. The amount of solid accrued at the cold vertical wall is clearly larger (resulting in 1986 solidified cells) and the melt/solid interface is clearly less curved than in the previous test cases. The isotherms (Fig. 5c) computed in the horizontal mid-plane (z = 0.5) show that the temperature field is practically two-dimensional. Identical results were obtained when applying the field in negative x-direction. In both cases the magnetic field force was surpressing vertical velocity components and consequently slowing the overall circulation..

4.4 Solidification with magnetic field in z-direction (against gravity):

In this case the magnetic field is acting upwards against the force of gravity. The computed isotherms (Fig.6a) in the vertical mid-plane (y = 0.5) are mildly curved as compared with the isotherms in the cases when the magnetic field was acting horizontally in y-direction (Fig. 4a) and in x-direction (Fig. 5a). The vertically upward magnetic field also suppresses the melt motion (Fig. 6b) and creates almost the same amount of solid on the cold vertical wall (there were 1962 solidified cells in this case) which is almost as much as in the case when the field was acting horizontally in the hot-to-cold direction. The melt/solid interface is also reminiscent of the shape obtained in the case when the field was acting horizontally in the hot-to-cold direction. The computed isotherms (Fig. 6c) in the horizontal mid-plane (z = 0.5) show that the temperature field in the melt is mildly three-dimensional. Identical results were obtained when applying the field in negative z-direction, that is, in the same direction as the gravity. In both cases the magnetic field force was surpressing horizontal velocity components and consequently slowing the overall circulation.

5. CONCLUSIONS

A mathematical model and a computer code have been developed for the simulation of solidification inside a closed container with an undercooled vertical and an externally applied steady magnetic field acting in an arbitrary direction. Computational results demonstrate clearly that the magnetic field reduces melt recirculation and consequently influences the temperature field and increases the amount of the solid accrued on the undercooled wall. It has been found that the application of the magnetic field in the direction perpendicular the plane of melt recirculation is most effective as far as suppressing the melt circulation, increasing the amount of solid accrued and reducing the curvature of the melt/solid interface. This demonstrates a feasibility for the development an inverse design and control algorithm that will automatically determine an optimal orientation and strength of the magnetic field in order to achieve a desired configuration of the melt/solid interface, minimize thermal gradients in the solid and maximize the solidification rate.

6. ACKNOWLEDGMENTS

The authors are grateful for the Cray-YMP computer time at NASA Ames Research Center NAS facility that was provided by Dr. L. Povinelli of NASA Lewis Research Center in Cleveland, Ohio and for the computer time at Cray Research, Inc. in Eagan, Minnesota that was provided by Mr. R. Vermeland and Mr. J. Dawson. The results were post processed at Penn State on equipment donated by Apple Computer, Inc. Useful references and comments were provided by Prof. Vaughan R. Voller and Prof. Gita Talmage and proofreading was performed by Mr. Thomas J. Martin.

7. REFERENCES

1. C. Vives, "Effects of a Magnetically Forced Convection During the Crystallization in Mould of Aluminum Alloys," *Journal of Crystal Growth*, Vol. 94, pp. 739-750, 1989.

2. H. Ozoe and K. Okada, "The Effect of the Direction of the External Magnetic Field on the Three-Dimensional Natural Convection in a Cubical Enclosure," *International Journal of Heat and Mass Transfer*, Vol. 32, No. 2, pp. 1939-1954, 1989.

3. S. Motakef, "Magnetic Field Elimination of Convective Interference With Segregation During Vertical-Bridgman Growth of Doped Semiconductors," *Journal of Crystal Growth*, Vol. 104, pp. 833-850, 1990.

4. G. S. Dulikravich, V. Ahuja and S. Lee, "Three-Dimensional Solidification With Magnetic Fields and Reduced Gravity," AIAA paper 93-0912, AIAA Aerospace Sciences Meeting, Reno, NV, Jan. 11-14, 1993.

5. G. S. Dulikravich, B. Kosovic and S. Lee, "Solidification in Reduced Gravity With Magnetic Fields and Temperature-Dependent Physical Properties," ASME WAM'91, Atlanta, GA, December 1-6, 1991, *Symposium on Heat and Mass Transfer in Solidification Processing*, Editors: S.G. Advani and C. Beckermann, HTD-Vol. 175/MD-Vol.25, pp. 61-73.

6. B. Kosovic, G. S. Dulikravich and S. Lee, "Freezing Under the Influence of a Magnetic Field: Computer Simulation," *Proceedings of ICHMT International Symposium on Macroscopic and Microscopic Heat & Mass Transfer in Biomedical Engineering*, Editors: K.Diller and A. Shitzer, Athens, Greece, Sept. 2-6, 1991, Elsevier Press, pp. 307-326.

7. G. S. Dulikravich and B. Kosovic, "Solidification of Variable Property Melts Under the Influence of Low Gravity, Magnetic Fields and Electric Fields," AIAA paper 92-0694, AIAA Aerospace Sciences Meeting, Reno, NV, Jan. 6-9,1992.

8. G. S. Dulikravich, B. Kosovic and S. Lee, "Magnetized Fiber Orientation Control in Solidifying Composites: Numerical Simulation," 28th ASME National Heat Transfer Conference, San Diego, CA., August 9-12, 1992, *Proceedings of the Symposium on Transport Phenomena in Materials Processing and Manufacturing*, Editors: M. Charmchi et al., HTD-Vol. 196, pp. 135-144; also to appear in *Journal of Heat Transfer*, Spring 1993.

9. O. M. Stuetzer, "Magnetohydrodynamics and Electrohydrodynamics," *The Physics of Fluids*, Vol. 5, No. 5 , pp. 534-544, 1962.

10. G. D. Robertson, Jr. and D. O'Connor, "Magnetic Field Effects on Float-Zone Si Crystal Growth II: Strong transverse fields," *Journal of Crystal Growth*, Vol. 76, pp. 100-110, 1986.

11. G. D. Robertson, Jr. and D. O'Connor, "Magnetic Field Effects on Float-Zone Si Crystal Growth III: Strong axial fields," *Journal of Crystal Growth*, Vol. 76, pp. 111-122, 1986.

12. M. Salcudean and P. Sabhapathy, "Numerical Study of Liquid Encapsulated Czochralski Growth of Gallium Arsenide with and without an Axial Magnetic Field," *Symposium on Computer Modeling and Simulation of Manufacturing Processes*, Editors: Singh, B., Im, Y. T., Haque, I. and Altan, C., ASME MD-Vol. 20, Book No. G00552, pp.115-127, 1990.

13. D. D. Gray and A. Giorgini, "The Validity of the Boussinesq Approximation for Liquids and Gases," *International Journal of Heat and Mass Transfer*, Vol. 19, pp. 545-551, 1976.

14. V. R. Voller and C. R. Swaminathan, "General Source-Based Method for Solidification Phase Change," *Numerical Heat Transfer, Part B*, Vol. 19, pp. 175-189, 1991.

15. J. A. Chorin, "A Numerical Method for Solving Incompressible Viscous Flow Problems," *Journal of Computational Physics*, Vol. 2, pp. 12-26, 1967.

16. S. Lee and G. S. Dulikravich, "Magnetohydrodynamic Steady Flow Computations in Three Dimensions," *Internat.Journal for Numerical Methods in Fluids*, Vol. 13, No. 8, pp. 917-936, Oct. 1991.

17. A. Jameson, W. Schmidt and E. Turkel, "Numerical Solution of the Euler Equations by Finite Volume Methods Using Runge-Kutta Time-Stepping Scheme," AIAA paper 81-1259, *Proceedings of AIAA Computational Fluid Dynamics Conference*, Palo Alto, CA, June 1981.

18. J. L. Duranceau and R. A. Brown, "Thermal-Capillary Analysis of Small-Scale Floating Zones: Steady-State Calculations," *Journal of Crystal Growth*, Vol. 75, pp. 367-389, 1986.

19. P. A. Sackinger, R. A. Brown and J. J. Derby, "A Finite Element Method for Analysis of Fluid Flow, Heat Transfer and Free Interfaces in Czochralski Crystal Growth," *International Journal for Numerical Methods in Fluids*, Vol. 9, pp. 453-492, 1989.

20. A. Mühlbauer, W. Erdmann and W. Keller, "Electrodynamic Convection in Silicon Floating Zones," *Journal of Crystal Growth*, Vol. 64, pp. 529-545, 1983.

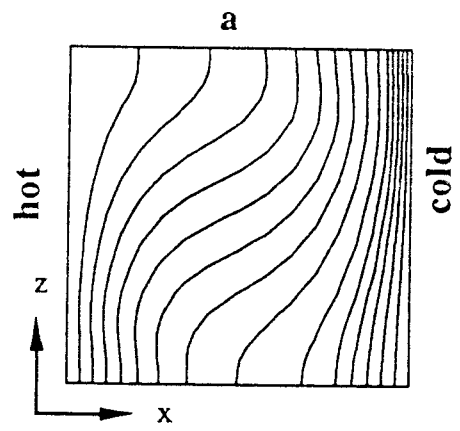

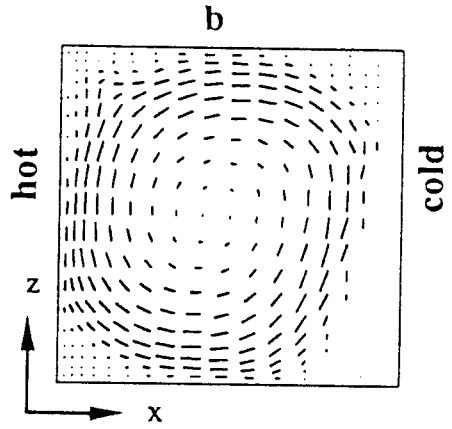

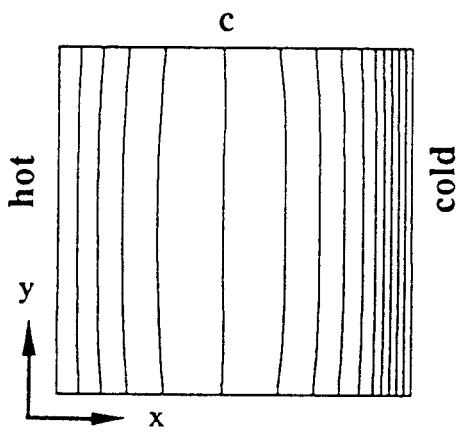

Fig. 3 Soldification with no magnetic field:
a) isotherms in vertical y = 0.5 mid-plane;
b) velocity vectors in vertical y = 0.5 mid-plane;
c) isotherms in horizontal z = 0.5 mid-plane.

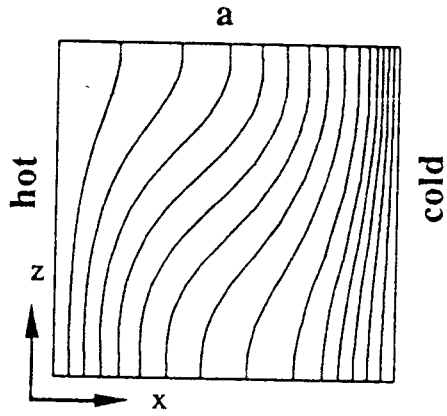

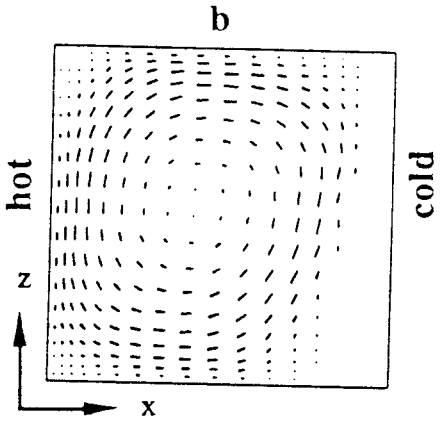

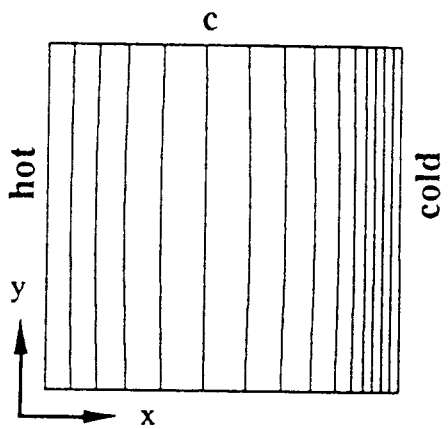

Fig. 4 Soldification with magnetic field in y-direction:
a) isotherms in vertical y = 0.5 mid-plane;
b) velocity vectors in vertical y = 0.5 mid-plane;
c) isotherms in horizontal z = 0.5 mid-plane.

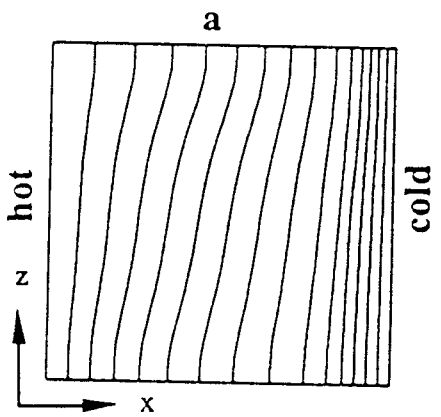

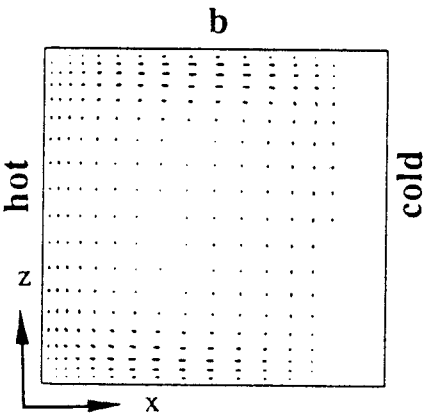

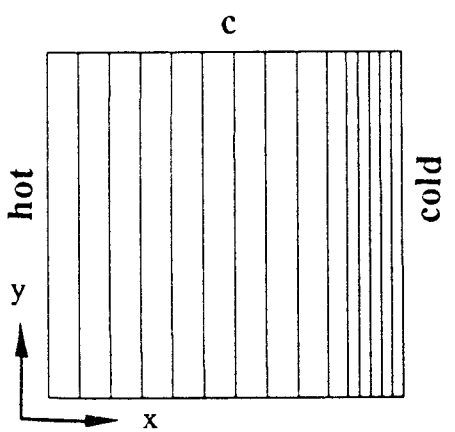

Fig. 5 Soldification with magnetic field in positive x-direction:
a) isotherms in vertical y = 0.5 mid-plane;
b) velocity vectors in vertical y = 0.5 mid-plane;
c) isotherms in horizontal z = 0.5 mid-plane.

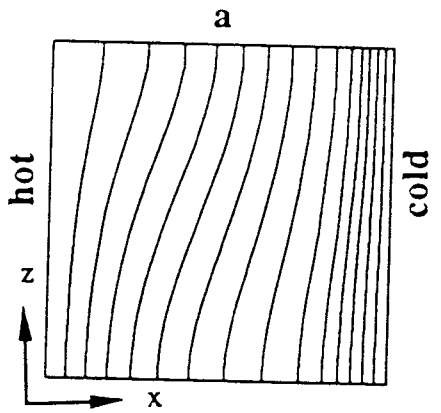

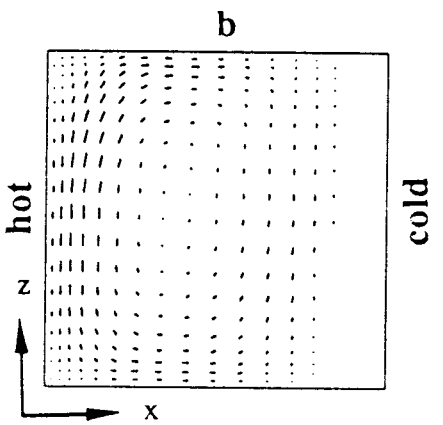

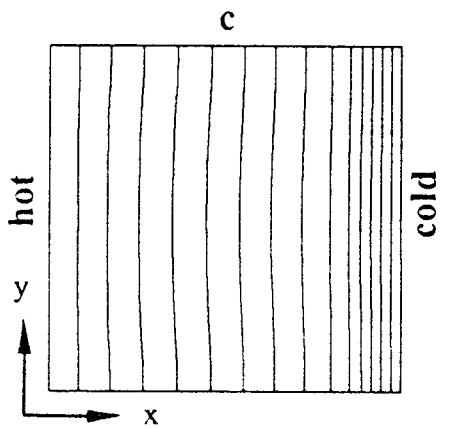

Fig. 6 Soldification with magnetic field in positive z-direction:
a) isotherms in vertical y = 0.5 mid-plane;
b) velocity vectors in vertical y = 0.5 mid-plane;
c) isotherms in horizontal z = 0.5 mid-plane.